Chapter

A New BEM for Modeling and Simulation of Laser Generated Ultrasound Waves in 3T Fractional Nonlinear Generalized Micropolar Poro-Thermoelastic FGA Structures

Mohamed Abdelsabour Fahmy

Abstract

In this chapter, we introduce a new theory called acoustic wave propagation of three-temperature fractional nonlinear generalized micropolar poro-thermoelasticity and we propose a new boundary element technique for modeling and simulation of laser-generated ultrasonic wave propagation problems of functionally graded anisotropic (FGA) structures which are linked with the proposed theory. Since it is very difficult to solve general acoustic problems of this theory analytically, we need to develop and use new computational modeling techniques. So, we propose a new boundary element technique for solving such problems. The numerical results are shown graphically to depict the effects of three temperatures on the thermal stress waves propagation. The validity, accuracy, and efficiency of our proposed theory and the technique are examined and demonstrated by comparing the obtained outcomes with those previously reported in the literature as special cases of our general study.

Keywords: boundary element method, modeling and simulation, laser ultrasonics, three-temperature, fractional-order, nonlinear generalized micropolar poro-thermoelasticity, functionally graded anisotropic structures

1. Introduction

The fractional calculus has recently been widely used to describe anomalous diffusion instead of classical diffusion, where the standard time derivative is replaced by fractional time derivative. Indeed, fractional calculus has important applications in electronics, wave propagation, nanotechnology, control theory, electricity, heat conduction modeling and identification, signal and image processing, biochemistry, biology, viscoelasticity, hereditary solid mechanics, and fluid dynamics.

Physically, according to the medium where the waves are transmitted, there are three wave types which are classified as mechanical waves, electromagnetic waves, and matter waves. Mechanical waves can travel through any medium with speed depending on elasticity and inertia and cannot travel through a vacuum. Electromagnetic waves can travel through a vacuum and do not need a medium to travel like X-ray, microwaves, ultraviolet waves, and radio waves. Matter waves are also called De Broglie waves that have wave-particle duality property. There are two mechanisms that have been proposed to explain wave generation, a first mechanism at high energy density, which leads to forces that generate ultrasound, and a second mechanism at low energy density, which generates elastic waves according to irradiation of laser pulses onto a material. The interaction between laser light and a metal surface led to great progress to develop theoretical models to describe the experimental data [1]. Scruby et al. [2] proved that the thermoelastic area source had been reduced to a surface point-source. This point-source ignores the optical absorption, the heat source thermal diffusion, and the limited side dimensions of the source. Based on point-source representation, Rose [3] introduced Surface Center of Expansion (SCOE) models which predict the major features of ultrasound waves generated by laser. Doyle [4] established that the existence of the metal precursor is due to subsurface sources which arise from thermal diffusion. According to McDonald [5], Spicer [6] used the generalized thermoelasticity theory to introduce a real circular laser source model taking into consideration spatial-temporal laser pulse design and thermal diffusion effect. The mathematical foundations of three-temperature were laid for nonlinear generalized thermoelasticity theory by Fahmy [7–12]. Fahmy [7] introduced a new boundary element strategy for modeling and simulation of three-temperature nonlinear generalized micropolar-magneto-thermoelastic wave propagation problems in FGA structures. Fahmy [8] proposed a boundary element formulation for three-temperature thermal stresses in anisotropic circular cylindrical plate structures. Fahmy [9] developed a boundary element model to describe the three-temperature fractional-order heat transfer in magneto-thermoelastic functionally graded anisotropic structures. Fahmy [10] introduced a boundary element formulation for modeling and optimization of micropolar thermoviscoelastic problems. Fahmy [11] discussed modeling and optimization of photo-thermoelastic stresses in three-temperature anisotropic semiconductor structures. Fahmy [12] proposed a new boundary element algorithm for nonlinear modeling and simulation of three-temperature anisotropic generalized micropolar piezothermoelasticity with memory-dependent derivative. This chapter differs from the references mentioned above, because it constructs a new acoustic wave propagation theory and allows the effective, efficient, and simple solution to the considered complex problems related with the proposed theory.

Recently, research on nonlinear generalized micropolar thermoelastic wave propagation problems has become very popular due to its practical applications in various fields such as astronautics, oceanology, aeronautics, narrow-band and broad-band systems, fiber-optic communication, fluid mechanics, automobile industries, aircraft, space vehicles, materials science, geophysics, petroleum and mineral prospecting, geomechanics, earthquake engineering, plasma physics, nuclear reactors, high-energy particle accelerators, and other industrial applications. Due to computational difficulties in solving nonlinear generalized micropolar poro-thermoelastic problems analytically, many numerical techniques have been developed and implemented for solving such problems [13, 14]. The boundary element method (BEM) [15–22] has been recognized as an attractive alternative numerical method to domain methods [23–26] like finite difference method (FDM), finite element method (FEM), and finite volume method (FVM) in engineering applications. The superior feature of BEM over domain methods is that it only needs to discretize the boundary, which often leads to fewer elements and easier to use. In the boundary element method (BEM) formulation, boundary integral equations involving singular integrands, the proper treatment of the singular integration has become essential in terms of numerical accuracy and efficiency of BEM. Also, some domain integrals may appear representing body forces, nonlinear effects, etc. Through our BEM solution, several approaches have been used to transform domain integrals into equivalent boundary integrals, so that the final boundary element formulation solution involves only the boundary integrals. The boundary element formulation of the current general study has been derived by using the weighted residual method [27–51]. In engineering applications, both FEM and BEM are based on the weighted residual methods with the same approximation procedure based on interpolation functions over each element to approximate the state variables distribution. Both methods differ in choosing the weighting functions. FEM as a domain method needs discretization of the whole domain, which usually leads to large systems of equations. This advantage of BEM over FEM has significant importance for modeling and simulation of thermal stress wave propagation problems which can be implemented using BEM with little cost and less input data. The solutions by BEM, like boundary thermal stress wave problems, are more accurate than by FEM, especially near the place of stress concentration. This feature is very important for our proposed theory and the technique of solving its related problems.

In this chapter, we introduce a novel theory called acoustic wave propagation of three-temperature fractional nonlinear generalized micropolar poro-thermoelasticity and we propose a new boundary element technique for modeling and simulation of laser-generated ultrasonic wave propagation problems of functionally graded anisotropic (FGA) structures which are linked with the proposed theory. Since it is very difficult to solve general acoustic problems of this theory analytically and we need to develop and use new computational modeling techniques. So, we propose a new boundary element technique for solving such problems. The numerical results are shown graphically to depict the effects of three temperatures on the propagation of thermal stresses waves. Since there are no available data for comparison with our proposed technique results, so, we replace the radiative heat conduction equations with heat conduction as a special case from our present general study. In the special case under consideration, the BEM results have been compared graphically with the FDM and FEM in the heat conduction and radiative heat conductions cases; it can be noticed that the BEM results are in a good agreement with the FDM and FEM results and thus demonstrate the validity and accuracy of our proposed theory and the technique used to solve its general problems.

A brief summary of the chapter is as follows: Section 1 introduces the background and provides the readers with the necessary information to books and articles for a better understanding of wave propagation problems in three-temperature nonlinear generalized micropolar poro-thermoelastic FGA structures and their applications. Section 2 describes the BEM modeling of the new theory and introduces the partial differential equations that govern its related problems. Section 3 outlines BEM simulation of temperature field. Section 4 discusses BEM simulation of micropolar porothermoelastic field to obtain the three temperatures thermal stress wave propagation. Section 5 presents the new numerical results that describe the thermal stress wave propagation under the effect of three-temperature on the FGA structures.

2. BEM modeling of the problem

We consider an anisotropic micropolar porous smart structure in a rectangular Cartesian system (x_1, x_2, x_3) shown in **Figure 1**, with a configuration R bounded by

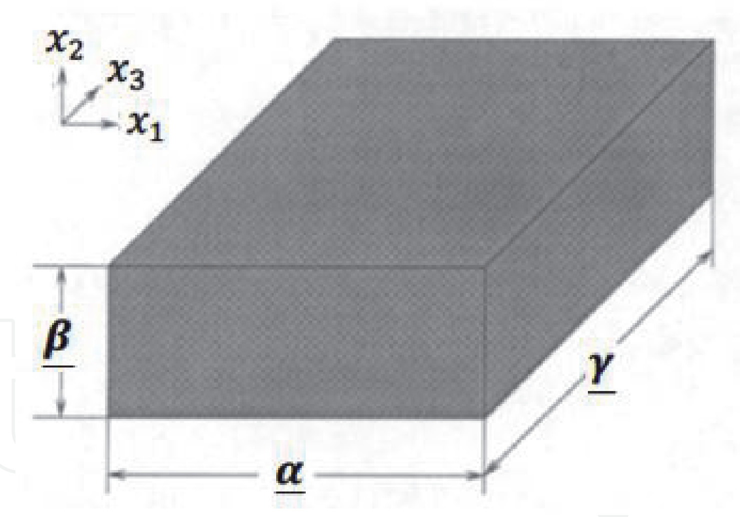

Figure 1.
Geometry of the FGA structure.

a closed surface S, and $S_i (i = 1, 2, 3, 4, 5, 6)$ denotes subsets of S such that $S_1 + S_2 = g_3 + S_4 = S_5 + S_6$. The governing equations for modeling of fractional three-temperature nonlinear generalized micropolar poro-thermoelastic problems of functionally graded anisotropic structures (FGA) can be expressed as [7].

$$\sigma_{ij,j} + \rho F_i = \rho \ddot{u}_i + \phi \rho_{\mathcal{F}} \ddot{v}_i \tag{1}$$

$$m_{ij,j} + \varepsilon_{ijk} \sigma_{jk} + \rho M_i = J \rho \ddot{\omega}_i \tag{2}$$

$$\dot{\zeta} + q_{i,i} = \mathbb{C} \tag{3}$$

where

$$\sigma_{ij} = (z \quad + 1)^m \left[C_{ijkl}\, e\delta_{ij} - A\delta_{ij} p + \breve{\alpha}\left(u_{j,i} - \varepsilon_{ijk}\omega_k\right) - \beta_{ij} T_\alpha \right] \tag{4}$$

$$C_{ijkl} = C_{klij} = C_{jikl}, \beta_{ij} = \beta_{ji} \tag{5}$$

$$m_{ij} = (x+1)^m \left[\alpha\, \omega_{k,k} \delta_{ij} + \overline{\alpha} \omega_{i,j} + \overline{\overline{\alpha}} = \omega_{\ j,i} \right] \tag{6}$$

$$\zeta = (x+1)^m \left[A u_{k,k} + \frac{\phi^2}{R} p \right] \tag{7}$$

$$q_i = (x+1)^m \left[-\overline{k} \left(p_{,i} + \rho_{\mathcal{F}} \ddot{u}_i + \frac{\rho_0 + \phi \rho_{\mathcal{F}}}{\phi} \ddot{v}_i \right) \right] \tag{8}$$

$$\epsilon_{ij} = \varepsilon_{ij} - \varepsilon_{ijk} (\chi + 1)^m (r_k - \omega_k) \tag{9}$$

$$\varepsilon_{ij} = \frac{1}{2} \left(u_{i,j} 1 + u_{j,i} \right) \tag{10}$$

$$r_i = \frac{1}{2} \varepsilon_{ikl} u_{l,k} \tag{11}$$

The time-fractional order three-temperature radiative heat conduction equations can be written as

$$D_\tau^a T_\alpha(r, \tau) = \xi \nabla [\mathbb{K}_\alpha \nabla T_\alpha(r, \tau)] + \xi \overline{\mathbb{W}}(r, \tau), \xi = \frac{1}{c_\alpha \rho \delta_1} \tag{12}$$

where

$$\overline{\mathbb{W}}(r,\ \ \tau)=\begin{cases}\rho\mathbb{W}_{ei}(T_e-T_i)+\rho\overline{\overline{\mathbb{W}}}_{er}\left(T_e-T_p\right)+\overline{\overline{\mathbb{W}}},\ \ \alpha=e,\ \ \delta_1=1\\ -\rho\mathbb{W}_{ei}(T_e-T_i)+\overline{\overline{\mathbb{W}}}, \qquad \alpha=i,\ \ \delta_1=1\\ -\rho\mathbb{W}_{er}\left(T_e-T_p\right)+\overline{\overline{\mathbb{W}}}, \qquad \alpha=p,\delta_1=T_p^3\end{cases} \tag{13}$$

$$\begin{aligned}\overline{\overline{\mathbb{W}}}(r,\tau)=&-\delta_{2n}\mathbb{K}_\alpha\dot{T}_{\alpha,ij}+\beta_{ij}T_{\alpha 0}\left[\text{Å}\delta_{1n}\dot{u}_{i,j}+(\tau_0+\delta_{2n})\ddot{u}_{i,j}\right]\\ &+\rho c_\alpha\left[(\tau_0+\delta_{1n^{T_2}}+\delta_{2n})\ddot{T}_\alpha\right]\end{aligned} \tag{14}$$

and

$$\mathbb{W}_{ei}=\rho\mathbb{A}_{ei}T_e^{-2/3},\ \ \mathbb{W}_{er}=\rho\mathbb{A}_{er}T_e^{-1/2},\ \ \mathbb{K}_\alpha=\mathbb{A}_\alpha T_\alpha^{5/2},\ \ \alpha=e,i,\ \ \mathbb{K}_p=\mathbb{A}_pT_p^{3+\mathbb{B}} \tag{15}$$

The total energy is

$$P=P_e+P_i+P_p,\ \ P_e=c_eT_e,\ \ P_i=c_iT_i,\ \ P_p=\frac{1}{4}c_pT_p^4 \tag{16}$$

where we considered that $\theta=T_e+T_i+T_r,\ T_e,\ \ T_i$, and T_r are temperature functions of electron, ion, and photon, respectively, $\mathbb{K}_e,\mathbb{K}_i$, and $\mathbb{K}_r$ are conductive coefficients of electron, ion, and photon, respectively, and ρ is the material density which is constant inside each subdomain.

3. BEM simulation for temperature field

In this section, we are interested in using a boundary element method for modeling the nonlinear time-dependent two dimensions three temperature (2D-3T) radiation heat equations coupled with electron, ion, and phonon temperatures.

According to finite difference scheme of Caputo at times $(f+1)\Delta\tau$ and $f\Delta\tau$, we obtain [52].

$$D_\tau^aT_\alpha^{f+1}+D_\tau^aT_\alpha^f\approx\sum_{j=0}^{k}W_{a,j}\left(T_\alpha^{f+1-j}(r)-T_\alpha^{f-j}(r)\right) \tag{17}$$

where

$$W_{a,0}=\frac{(\Delta\tau)^{-a}}{\Gamma(2-a)},\ \ W_{a,j}=W_{a,0}\left((j+1)^{1-a}-(j-1)^{1-a}\right) \tag{18}$$

Based on Eq. (17), the fractional order heat Eq. (12) can be replaced by the following system

$$\begin{aligned}&W_{a,0}T_\alpha^{f+1}(r)-\mathbb{K}_\alpha(x)T_{\alpha,II}^{f+1}(r)-\mathbb{K}_{\alpha,I},(x)T_{\alpha,I}^{f+1}(r)\\ &\qquad=W_{a,0}T_\alpha^f(r)-\mathbb{K}_\alpha(x)T_{\alpha,II}^f(r)\\ &-\mathbb{K}_{\alpha,I},(x)T_{\alpha,J]}^f(r)-\sum_{j=1}^{f}W_{a,j}\left(T_\alpha^{f+1-j}(r)-T_\alpha^{f-j}(r)\right)+\overline{\mathbb{W}}_m^{f+1}(x,\tau)\\ &\qquad+\overline{\mathbb{W}}_m^f(x,\tau)\end{aligned} \tag{19}$$

where, $j = 1, 2, \ldots, F,\ f = 0, 1, 2, \ldots, F$.

Now, according to Fahmy [9] and using the fundamental solution that satisfies the system (19), the boundary integral equations corresponding to (12) without internal heat sources can be written as

$$CT_\alpha = \int_s \left[T_\alpha q^* - T_\alpha^* q\right] dS - \int_R \frac{\mathbb{K}_\alpha}{D} \frac{\partial T_\alpha^*}{\partial \tau} T_\alpha dR \tag{20}$$

Now, to transform the domain integral in (20) into the boundary, we assume that the time-temperature derivative can be approximated by using a series of known functions $f^j(r)$ and unknown coefficients $a^j(\tau)$ as

$$\frac{\partial T_\alpha}{\partial \tau} \cong \sum_{j=1}^{N} f^j(r)^j a^j(\tau) \tag{21}$$

We assume that $\hat{T}_\alpha^j$ is a solution of

$$\nabla^2 \hat{T}_\alpha^j = f^j \tag{22}$$

Thus, Eq. (20) can be written as

$$\begin{aligned} CT_\alpha = & \int_S \left[T_\alpha q^* - T_\alpha^* q\right] dS \\ & + \sum_{j=1}^{N} a^j(\tau) D^{-1} \left(C\hat{T}_\alpha^j - \int_S \left[T_\alpha^j q^* - \hat{q}^j T_\alpha^*\right] dS \right) \end{aligned} \tag{23}$$

where

$$\hat{q}^j = -\mathbb{K}_\alpha \frac{\partial \hat{T}_\alpha^j}{\partial n} \tag{24}$$

and

$$a^j(\tau) = \sum_{i=1}^{N} f_{ji}^{-1} \frac{\partial T(r_i, \tau)}{\partial \tau} \tag{25}$$

In which, the entries of f_{ji}^{-1} are the coefficients of F^{-1} with matrix F defined as

$$\{F\}_{ji} = f^j(r_i) \tag{26}$$

Using the standard boundary element discretization scheme [28], for Eq. (23) and using Eq. (25), we get

$$C\dot{T}_\alpha + HT_\alpha = GQ \tag{27}$$

where the matrices H and G are depending on current time step, boundary geometry, and material properties.

The diffusion matrix can be defined as

$$C = -\left[H\hat{T}_\alpha - G\hat{Q}\right] F^{-1} D^{-1} \tag{28}$$

with

$$\{\hat{T}\}_{ij} = \hat{T}^j(x_i) \tag{29}$$

$$\{\hat{Q}\}_{ij} = \hat{q}^j(\chi_i) \tag{30}$$

In order to solve Eq. (27) numerically, the functions T_α and q are interpolated as

$$T_\alpha = (1-\theta)T_\alpha^m + \theta T_\alpha^{m+1} \tag{31}$$

$$q = (1-\theta)q^m + \theta q^{m+1} \tag{32}$$

The time derivative of the temperature can be written as

$$\dot{T}_\alpha = \frac{dT_\alpha}{d\theta}\frac{d\theta}{d\tau} = \frac{T_\alpha^{m+1} - T_\alpha^m}{\tau^{m+1} - \tau^m} = \frac{T_\alpha^{m+1} - T_\alpha^m}{\Delta\tau^m}, \quad \theta = \frac{\tau - \tau^m}{\tau^{m+1} - \tau^m}, 0 \le \theta \le 1 \tag{33}$$

By substituting from Eqs. (31)–(33) into (27), we obtain

$$\left(\frac{c}{\Delta\tau^m} + \theta H\right)T_\alpha^{m+1} - \theta G Q^{m+1} = \left(\frac{c}{\Delta\tau^m} - (1-\theta)H\right)T_\alpha^m + (1-\theta)GQ^m \tag{34}$$

which can be written as follows [10].

$$\mathbb{a}X = \mathbb{b} \tag{35}$$

where $\mathbb{a}$ is an unknown matrix, while $\mathbf{X}$ and $\mathbb{b}$ are known matrices.

The explicit staggered predictor-corrector procedure based on communication-avoiding Arnoldi (CA-Arnoldi) method [53] due to its numerical stability, convergence, and performance [7] has been implemented for obtaining the temperature field in terms of predicted displacement field which will be explained in the next section.

4. BEM simulation for micropolar poro-thermoelastic fields

By implementing the weighted residual method, the governing Eqs. (1)–(3) can be written as

$$\int_R (\sigma_{ij,j} + U_i)u_i^* \, dR = 0 \tag{36}$$

$$\int_R (m_{ij,j} + \varepsilon_{ijk}\sigma_{jk} + V_i)\omega_i^* \, dR = 0 \tag{37}$$

$$\int_R (q_i + \dot{\zeta}_i - \mathbb{C}_i)p_i^* \, dR = 0 \tag{38}$$

in which

$$U_i = \varphi_{ij_j} + \rho F_i - \rho\ddot{u}_i - \phi\rho_{\mathcal{F}}\ddot{v}_i \tag{39}$$

$$V_i = \rho(M_i - J\ddot{\omega}_i) \tag{40}$$

where u_i^*, ω_i^* and p_i^* are weighting functions, u_i, ω_i, and p_i are approximate solutions as shown in Eqs. (4)–(11)

The boundary conditions are

$$u_i = \overline{u}_i \qquad \text{on}\, S_1 \tag{41}$$

$$\lambda_i = \sigma_{ii} n_i = \overline{\lambda}_i \qquad \text{on}\, S_2 \tag{42}$$

$$\omega_i = \overline{\omega}_i \qquad \text{on}\, S_3 \tag{43}$$

$$\mu_i = m_{ij} n_j = \overline{\mu}_i \qquad \text{on}\, S_4 \tag{44}$$

$$p = \overline{p} \qquad \text{on}\, S_5 \tag{45}$$

$$L = \frac{\partial p}{\partial n} = \overline{L} \qquad \text{on}\, S_6 \tag{46}$$

By integrating by parts the first term of Eqs. (36)–(38), we obtain

$$-\int_R \sigma_{ij} u^*_{i,j}\, dR + \int_R U_i u^*_i\, dR = -\int_{S_2} \lambda_i u^*_i\, dS \tag{47}$$

$$\begin{aligned} &-\int_R m_{ij}\omega^*_{i,j}\, dR + \int_R \varepsilon_{ijk}\sigma_{jk}\omega^*_i\, dR + \int_R V_i \omega^*_i\, dR \\ &\quad = -\int_{S_4} \mu_i \omega^*_i\, dS \end{aligned} \tag{48}$$

$$-\int_R q\, \mathrm{p}^*_{i,i}\, dR + \int_R \dot{\zeta}_i \mathrm{p}^*_i\, dR - \int_R \mathbb{C}_i\, \mathrm{p}^*_i\, dR = -\int_{S_6} L_i \mathrm{p}^*_i\, dS \tag{49}$$

which according to Huang and Liang [54] can be expressed as

$$\begin{aligned} &-\int_R \sigma_{ij,j} u^*_i\, dR + \int_R (m_{ij,j} + \varepsilon_{ijk}\sigma_{jk})\omega^*_i\, dR + \int_R U_i u^*_i\, dR \\ &\quad + \int_R V_i \omega^*_i\, dR - \int_R q\, \mathrm{p}^*_{i,i} dR + \int_R \dot{\zeta}_i \mathrm{p}^*_i\, dR - \int_R \mathbb{C}_i\, \mathrm{p}^*_i\, dR \\ &\quad = \int_{S_2} (\lambda_i - \overline{\lambda}_i) u^*_i\, dS + \int_{S_1} (\overline{u}_i - u_i)\lambda^*_i\, dS \\ &\quad + \int_{S_4} (\mu_i - \overline{\mu}_i)\omega^*_i\, dS + \int_{S_3} (\overline{\omega}_i - \omega_i)\mu^*_i\, dS \\ &\quad + \int_{S_6} (L_i - \overline{L}_i)\mathrm{p}^*_i\, dS + \int_{S_5} (\overline{\mathrm{p}}_i - \mathrm{p}_i) L^*_i\, dS \end{aligned} \tag{50}$$

Using integration by parts for the left-hand side of (50), we have

$$\begin{aligned} &-\int_R \sigma_{ij}\varepsilon^*_{ij}\, dR - \int_R m_{ij,j}\omega^*_{i,j}\, dR + \int_R U_i u^*_i\, dR \\ &\quad + \int_R V_i \omega^*_i\, dR - \int_R q\, \mathrm{p}^*_{i,i} dR + \int_R \dot{\zeta}_i \mathrm{p}^*_i\, dR - \int_R \mathbb{C}_i \mathrm{p}^*_i\, dR \\ &\quad = -\int_{S_2} \overline{\lambda}_i u^*_i\, dS - \int_{S_1} \lambda_i u^*_i\, dS \\ &\quad + \int_{S_1} (\overline{u}_i - u_i)\lambda^*_i\, dS - \int_{S_4} \overline{\mu}_i \omega^*_i\, dS - \int_{S_3} \mu \omega^*_i\, dS \\ &\quad + \int_{S_3} (\overline{\omega}_i - \omega_i)\mu^*_i\, dS - \int_{S_6} \overline{L}_i\, \mathrm{p}^*_i\, dS - \int_{S_6} L_i \mathrm{p}^*_i\, dS \\ &\quad + \int_{S_5} (\overline{\mathrm{p}}_i - \mathrm{p}_i) L^*_i\, dS \end{aligned} \tag{51}$$

By using the following elastic stress and couple stress (see Eringen [55])

$$\sigma_{ij} = \mathbb{A}_{ijkl}\,\varepsilon_{kl},\;\; m_{ij} = \mathbb{B}_{ijkl}\,\omega_{k,l} \text{ where } \mathbb{A}_{ijkl} = \mathbb{A}_{klij} \text{ and } \mathbb{B}_{ijkl} = \mathbb{B}_{klij} \tag{52}$$

Hence, Eq. (51) can be rewritten as

$$\begin{aligned} &-\int_R \sigma_{ij}^* \varepsilon_{ij} dR - \int_R m_{ij,j}^* \omega_{i,j} dR + \int_R U_i u_i^*\, dR \\ &\quad + \int_R V_i \omega_i^*\, dR - \int_R q\, \mathrm{p}_{i,i}^* dR + \int_R \dot{\zeta}_i\, \mathrm{p}_i^*\, dR - \int_R \mathbb{C}_i\, \mathrm{p}_i^*\, dR \\ &\quad = -\int_{S_2} \overline{\lambda}_i u_i^*\, dS - \int_{S_1} \lambda_i u_i^*\, dS \\ &\quad + \int_{S_1} (\overline{u}_i - u_i)\lambda_i^*\, dS - \int_{S_4} \overline{\mu}_i \omega_i^*\, dS - \int_{S_3} \mu_i \omega_i^*\, dS \\ &\quad + \int_{S_3} (\overline{\omega}_i - \omega_i)\mu_i^*\, dS - \int_{S_6} \overline{L}_i\, \mathrm{p}_i^*\, dS - \int_{S_6} L_i\, \mathrm{p}_i^*\, dS \\ &\quad + \int_{S_5} (\overline{\mathrm{p}}_i - \mathrm{p}_i) L_i^*\, dS \end{aligned} \tag{53}$$

Applying the integration by parts for the left-hand side of Eq. (53), we get

$$\begin{aligned} &\int_R \sigma_{ij,j}^* u_i\, dR + \int_R \left(m_{ij,j}^* + \varepsilon_{ijk}\sigma_{jk}^* \right)\omega_i dR \\ &\quad = -\int_S u_i^*\, \lambda_i\, dS - \int_S \omega_i^*\, \mu_i\, dS - \int_S \mathrm{p}_i^*\, L_i\, dS + \int_S \lambda_i^*\, u_i\, dS \\ &\quad + \int_S \mu_i^*\, \omega_i\, dS + \int_S L_i^*\, \mathrm{p}_i\, dS \end{aligned} \tag{54}$$

The weighting functions for $U_i = \Delta^n$ and $\mathrm{V_i} = 0$ along the unit vector direction e_l are as follows:

$$\sigma_{lj,j}^* + \Delta^n e_l = 0 \tag{55}$$

$$m_{ij,j}^* + \varepsilon_{ijk}\sigma_{jk}^* = 0 \tag{56}$$

The analytical fundamental solution of Dragos [56] can be written as

$$\begin{aligned} &u_i^* = u_{li}^*\, e_l, \omega_i^* = \omega_{li}^*\, e_l, p_i^* = p_{li}^* e_l,\;\; \lambda_i^* = \lambda_{li}^*\, e_l, \\ &\mu_i^* = \mu_{li}^* e_l,\;\; L_i^* = L_{li}^* e_l \end{aligned} \tag{57}$$

The obtained weighting functions for a point load $U_\mathrm{i} = 0$ and $V_i = \Delta^n$ along the unit vector direction e_1 were next used as follows:

$$\sigma_{ij,j}^{**} = 0 \tag{58}$$

$$m_{lj,j}^{**} + \varepsilon_{ljk}\sigma_{jk}^{**} + \Delta^n e_l = 0 \tag{59}$$

According to Dragos [56], the fundamental solution can be expressed as

$$\begin{aligned} &u_i^* = u_{ii}^{**}\, e_l,\;\; \omega_i^* = \omega_{li}^*\, e_l,\;\; p_i^* = p_{li}^{**}\, e_l,\;\; \lambda_i^* = \lambda_{li}^{**}\, e_l, \\ &\mu_i^* = \mu_{li}^*\, e_l,\;\; L_i^* = L_{li}^{**}\, e_l \end{aligned} \tag{60}$$

Using the weighting functions of (57) and (60) into (54), we obtain

$$\begin{aligned} C^n_{li}u^n_i &= -\int_S \lambda^*_{li}\, u_i dS - \int_S \mu^*_{li}\ \omega_i\, dS - \int_S \mathrm{L}^*_{li}\, p_i dS + \int_S u^*_{li}\, \lambda_i dS \\ &+ \int_S\ \omega^*_{li}\, \mu_i\, dS + \ \int_S p^*_{li}\, \mathrm{L}_i\, dS \end{aligned} \tag{61}$$

$$\begin{aligned} C^n_{li}\omega^n_i &= -\int_S \lambda^{**}_{li}\, u_i dS - \int_S \mu^{**}_{li}\ \omega_i\, dS - \int_S \mathrm{L}^{**}_{li}\, p_i dS + \int_S u^{**}_{li}\, \lambda_i dS \\ &+ \int_S\ \omega^{**}_{li}\, \mu_i\, dS + \ \int_S p^{**}_{li}\, \mathrm{L}_i\, dS \end{aligned} \tag{62}$$

Thus, we can write

$$C^n \mathbb{q}^n = -\int_S \mathbb{p}^*\, \mathbb{q}\, dS + \int_S \mathbb{q}^*\, \mathbb{p}^{dS+} \int_S \mathbb{a}^*\, p\, dS + \int_S \mathbb{b}^*\, \frac{\partial p}{\partial n} dS \tag{63}$$

where

$$C^n = \begin{bmatrix} C_{11} & C_{12} \\ C_{21} & C_{22} \end{bmatrix}, \mathbb{q}^* = \begin{bmatrix} u^*_{11} & u^*_{12} & \omega^*_{13} \\ u^*_{21} & u^*_{22} & \omega^*_{23} \\ u^*_{31} & u^*_{32} & \omega^*_{33} \end{bmatrix}, \mathbb{p}^* = \begin{bmatrix} \lambda^*_{11} & \lambda^*_{12} & \lambda^*_{13} \\ \lambda^*_{21} & \lambda^*_{22} & \mu^*_{23} \\ \lambda^*_{31} & \lambda^*_{32} & \mu^*_{33} \end{bmatrix} \tag{64}$$

$$\mathbb{q} = \begin{bmatrix} u_1 \\ u_2 \\ \omega_3 \end{bmatrix}, \mathbb{p} = \begin{bmatrix} \lambda_1 \\ \lambda_2 \\ \mu_3 \end{bmatrix}, \mathbb{a}^* = \begin{bmatrix} \mathbb{a}^*_1 \\ \mathbb{a}^*_2 \\ 0 \end{bmatrix}, \mathbb{b}^* = \begin{bmatrix} \mathbb{b}^*_1 \\ \mathbb{b}^*_2 \\ 0 \end{bmatrix}$$

In order to obtain the numerical solution of (63), we define the following functions

$$\mathbb{q} = \psi\, \mathbb{q}^j, \mathrm{p} = \psi \mathbb{p}^j, p = \psi_0 p^j, \frac{\partial p}{\partial n} = \psi_0 \left(\frac{\partial p}{\partial n}\right)^j \tag{65}$$

substituting above functions into (63) and discretizing the boundary, we obtain

$$\begin{aligned} C^n \mathrm{q}^n &= \sum_{j=1}^{N_e} \left[-\int_{\Gamma_j} \mathrm{p}^*\, \psi d\Gamma \right] \mathrm{q}^j + \sum_{j=1}^{N_e} \left[\int_{\Gamma_j} \mathrm{q}^*\, \psi d\Gamma \right] \mathrm{p}^j \\ &+ \sum_{j=1}^{N_e} \left[\int_{\Gamma_j} \mathrm{a}^*\, \psi_0\, d\Gamma \right] p^j + \sum_{j=1}^{N_e} \left[-\int_{\Gamma_j} \mathrm{b}^*\, \psi_0 d\Gamma \right] \left(\frac{\partial p}{\partial n}\right)^j \end{aligned} \tag{66}$$

Equation after integration can be written as

$$C^i \mathrm{q}^i = -\sum_{j=1}^{N_e} \hat{\mathbb{H}}^{ij} \mathrm{q}^j + \sum_{j=1}^{N_e} \hat{\mathrm{G}}^{ij} \mathrm{p}^j + \sum_{j=1}^{N_e} \hat{\mathrm{a}}^{ij} p^j + \sum_{j=1}^{N_e} \hat{\mathrm{b}}^{ij} \left(\frac{\partial p}{\partial n}\right)^j \tag{67}$$

By using the following representation

$$\mathbb{H}^{ij} = \begin{cases} \hat{\mathbb{H}}^{ij} & if\ \ i \neq j \\ \hat{\mathbb{H}}^{ij} + C^i & if\ \ i = j \end{cases} \tag{68}$$

Thus, we can write (67) as follows

$$\sum_{j=1}^{N_e} \mathbb{H}^{ij} \mathrm{q}^j = \sum_{j=1}^{N_e} \hat{\mathrm{G}}^{ij} \mathrm{p}^j + \sum_{j=1}^{N_e} \hat{\mathrm{a}}^{ij} p^j + \sum_{j=1}^{N_e} \hat{\mathrm{b}}^{ij} \left(\frac{\partial p}{\partial n}\right)^j \tag{69}$$

The global matrix system equation for all $\boldsymbol{i}$ nodes can be written as follows

$$\mathbb{HQ} = \mathbb{GP} + \mathbb{ai} + \mathbb{bj} \tag{70}$$

the vector $\mathbb{Q}$ represents all the values of displacements and microrotations, the vector $\mathbb{P}$ represents all the tractions and couple stress vector, the vector $\mathbb{i}$ represents all the values of pore pressure, and the vector $\mathbb{j}$ represents all the values of pore pressure gradients before applying boundary conditions.

Substituting the boundary conditions into (70), we obtain the following system of equations

$$\mathbb{AX} = \mathbb{B} \tag{71}$$

where $\mathbb{A}$ is an unknown matrix, while $\mathbb{X}$ and $\mathbb{B}$ are known matrices.

Now, an explicit staggered predictor-corrector procedure based on communication-avoiding Arnoldi (CA-Arnoldi) method has been implemented in (71) for obtaining the corrected displacement. Then we can get the temperature field from (35).

5. Numerical results and discussion

In order to show the numerical results of this study, we consider a monoclinic graphite-epoxy as an anisotropic micropolar poro-thermoelastic material which has the following physical constants.

The elasticity tensor is expressed as

$$C_{pjkl} = \begin{bmatrix} 430.1 & 130.4 & 18.2 & 0 & 0 & 201.3 \\ 130.4 & 116.7 & 21.0 & 0 & 0 & 70.1 \\ 18.2 & 21.0 & 73.6 & 0 & 0 & 2.4 \\ 0 & 0 & 0 & 19.8 & -8.0 & 0 \\ 0 & 0 & 0 & -8.0 & 29.1 & 0 \\ 201.3 & 70.1 & 2.4 & 0 & 0 & 147.3 \end{bmatrix} \mathrm{GPa} \tag{72}$$

The mechanical temperature coefficient is

$$\beta_{pj} = \begin{bmatrix} 1.01 & 2.00 & 0 \\ 2.00 & 1.48 & 0 \\ 0 & 0 & 7.52 \end{bmatrix} \cdot 10^6 \frac{\mathrm{N}}{\mathrm{km}^2} \tag{73}$$

The thermal conductivity tensor is

$$k_{pj} = \begin{bmatrix} 5.2 & 0 & 0 \\ 0 & 7.6 & 0 \\ 0 & 0 & 38.3 \end{bmatrix} \mathrm{W/Km} \tag{74}$$

Mass density $\rho = 7820\ \mathrm{kg/m^3}$ and heat capacity $c = 461\,\mathrm{J/kg\,K}$.

The proposed technique that has been utilized in the present chapter can be applicable to a wide variety of wave propagation of fractional nonlinear generalized micropolar poro-thermoelastic FGA structures problems related with the proposed theory.

The influence of three-temperature on the propagation of thermal stress waves plays a very important role during the simulation process. According to Fahmy [7], who compared and implemented communication-avoiding GMRES (CA-GMRES) of Saad and Schultz [57], communication-avoiding Arnoldi (CA-Arnoldi) of the Arnoldi [58] and communication-avoiding Lanczos (CA-Lanczos) of Lanczos [59] for solving the dense nonsymmetric algebraic system of linear equations arising from the BEM. So, the efficiency of the proposed technique has been developed using the communication-avoiding Arnoldi (CA-Arnoldi) solver to reduce the iterations number and CPU time, where the BEM discretization is employed 1280 quadrilateral elements, with 3964° of freedom (DOF).

Now, in order to assess the impact of three temperatures on the thermal stress waves, the numerical outcomes are completed and delineated graphically for electron, ion, and phonon temperatures.

Figures 2–**4** show the propagation of the thermal stress σ_{11}, σ_{12}, and σ_{22} waves along x-axis for the three temperatures T_e, T_i, and T_p and total temperature T. It was noted from these figures that the three temperatures have significant effects on the thermal stress waves along x-axis through the thickness of the FGA structure.

Since there are no available results for our considered problem. So, some literatures may be considered as special cases from our considered complex problem. For comparison purposes with the special cases of other methods treated by other authors, we only considered one-dimensional numerical results of the considered problem. In the special case under consideration, the BEM results have been plotted in **Figures 5** and **6** with the results of finite difference method (FDM) and finite element method (FEM) in the two cases, namely, three-temperature (3T) theory and one-temperature (1T) theory.

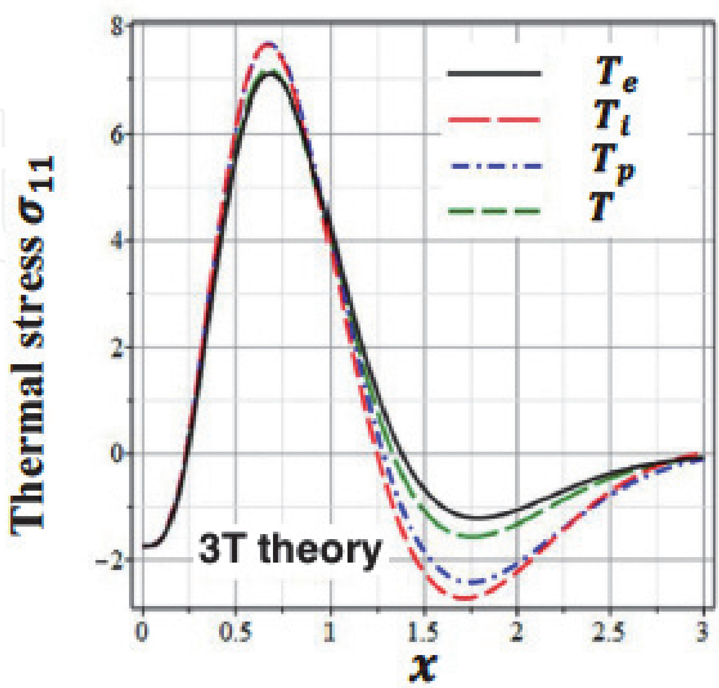

Figure 2.
Propagation of the thermal stress $\boldsymbol{\sigma_{11}}$ *waves along* $\mathbf{x}$*-axis for the three temperatures* T_e, T_i , T_p *and total temperature* T.

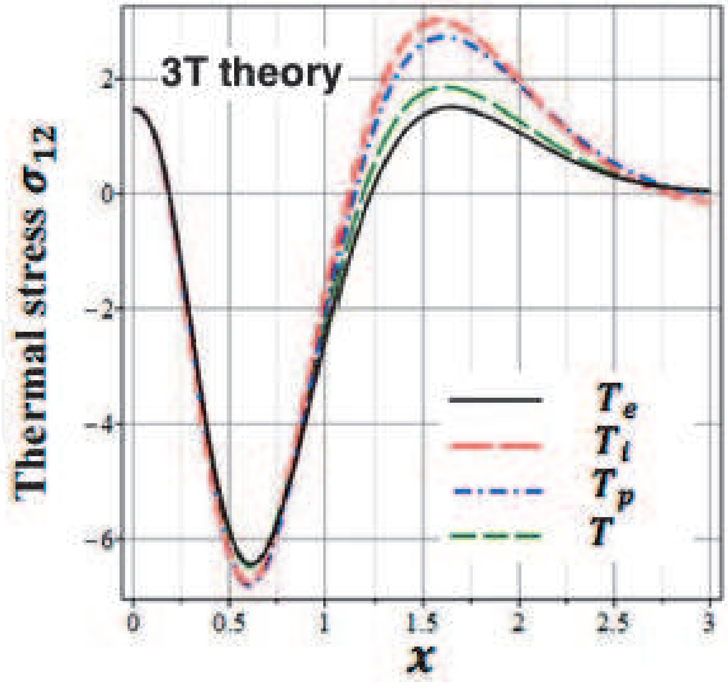

Figure 3.
Propagation of the thermal stress σ_{12} waves along x-axis for the three temperatures T_e, T_i, T_p and total temperature T.

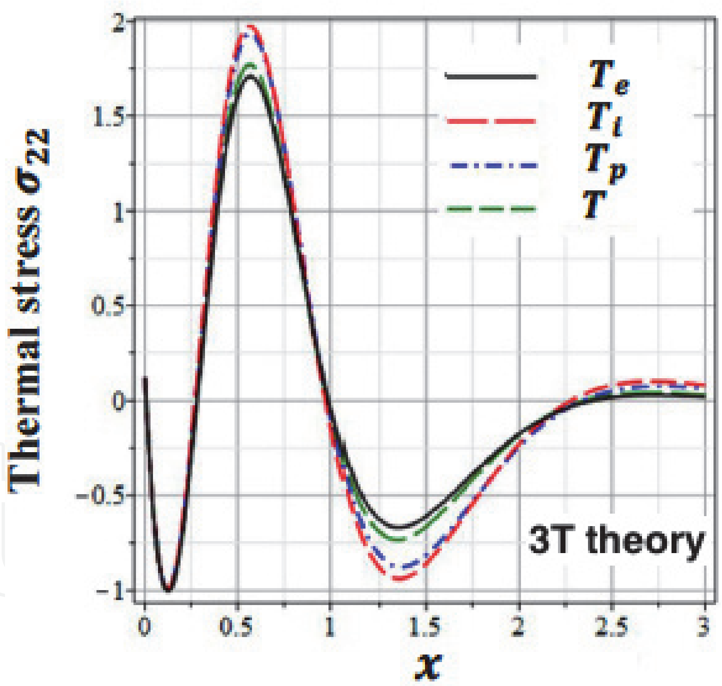

Figure 4.
Propagation of the thermal stress σ_{22} waves along x-axis for the three temperatures T_e, T_i, T_p and total temperature T.

Figure 5 shows a comparison of the propagation of the thermal stress σ_{11} waves for the BEM results of three-temperature (3T) radiative heat conduction theory for the BEM results with those obtained using the FDM of Pazera and Jędrysiak [60] and FEM of Xiong and Tian [61], where we replaced the 1T heat conduction theory of their work by 3T radiative heat conduction theory of our work to obtain the results. It can be noticed that the BEM results are found to agree very well with the FDM and FEM results.

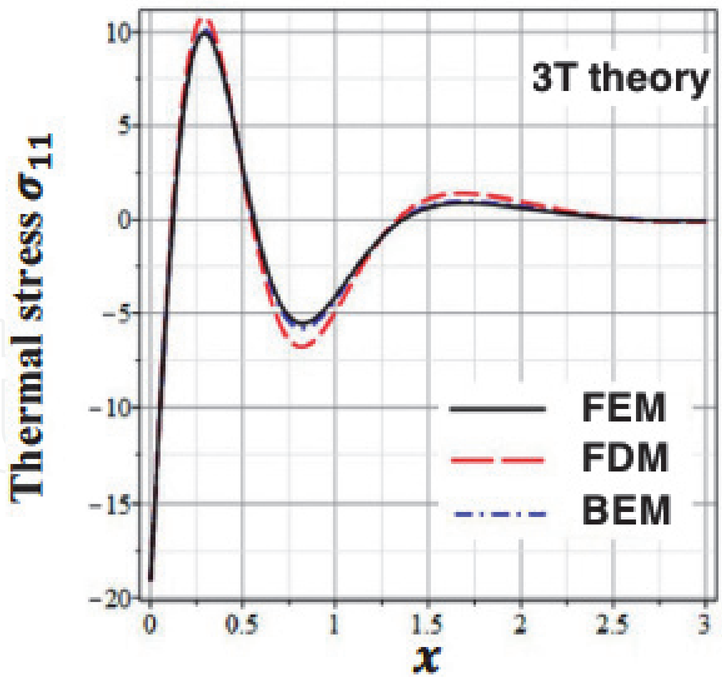

Figure 5.
Propagation of the thermal stress σ_{11} waves along x-axis for 3T theory and different methods.

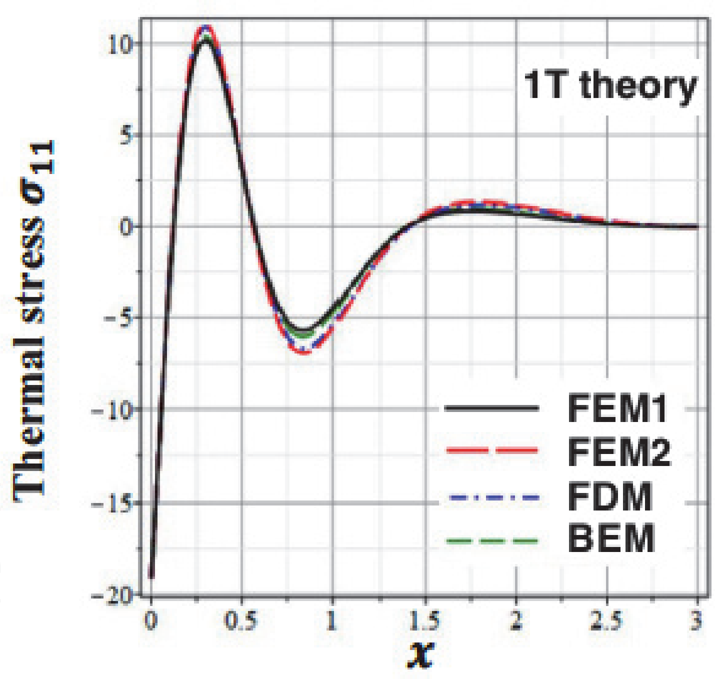

Figure 6.
Propagation of the thermal stress σ_{11} waves along x-axis for 1T theory and different methods.

Figure 6 shows a comparison of the propagation of the thermal stress σ_{11} waves for the BEM results of one-temperature (1T) heat conduction theory with those obtained using FDM of Pazera and Jędrysiak [60], FEM1 of Xiong and Tian [61], and FEM2 of COMSOL multiphysics software version 5.1, where we replaced 3T radiative heat conduction theory of our work by the 1T heat conduction theory of their work to obtain the results. It can be noticed that the BEM results are found to agree very well with the FDM, FEM1, and FEM2 results and thus demonstrate the validity and accuracy of our proposed theory and the technique used to solve its general problems.

6. Conclusion

The main purpose of this chapter is to introduce a novel theory called acoustic wave propagation of three-temperature fractional nonlinear generalized micropolar poro-thermoelasticity and we propose a new boundary element technique for modeling and simulation of ultrafast laser-induced thermal stress waves propagation problems in 3T nonlinear generalized micropolar poro-thermoelastic FGA structures which are linked with the proposed theory. By discretizing only, the boundary of the domain using BEM, where the unknowns on the domain boundary are expressed as functions depend only on the domain boundary values. Since it is very difficult to solve general acoustic problems of this theory analytically and we need to develop and use new computational modeling techniques. So, we propose a new boundary element technique for solving such problems. The numerical results are shown graphically to depict the effects of three temperatures on the thermal stress waves. Because there are no available results for comparison with the results of our proposed technique, we replace the three-temperature radiative heat conduction with one-temperature heat conduction as a special case from our present general study of three-temperature nonlinear generalized micropolar poro-thermoelasticity. In the special case under consideration, the BEM results have been compared graphically with the FDM and FEM in the two cases, namely three-temperature (3T) theory and one-temperature (1T) theory; it can be noticed that the BEM results are in a good agreement with the FDM and FEM results and thus demonstrate the validity and accuracy of our proposed theory and the technique used to solve its general problems. The numerical simulations are often faster and cheaper than experiments, and they are easily cross-platform, reproducible, relocatable, and customizable. So, the validation of the numerical simulation is of paramount importance. In this work, we implemented the explicit staggered predictor-corrector procedure based on communication-avoiding Arnoldi (CA-Arnoldi) solver due to its numerical stability, convergence, and performance as in Fahmy [10] to demonstrate the efficiency of the proposed technique. Thus, the numerical results of our proposed technique demonstrate the validity, accuracy, and efficiency of our proposed technique.

Nowadays, the knowledge of thermal stress wave propagation in three-temperature nonlinear generalized micropolar poro-thermoelastic problems associated with the ultrafast laser pulse proposed theory can be utilized by mechanical engineers in ceramic production applications and designing of boiler tubes and heat exchangers. As well as for chemists to observe the chemical reaction phenomena such as bond formation and bond breaking.

Author details

Mohamed Abdelsabour Fahmy
Faculty of Computers and Informatics, Suez Canal University, Ismailia, Egypt

*Address all correspondence to: mohamed_fahmy@ci.suez.edu.eg

References

[1] White R. Generation of elastic waves by transient surface heating. Journal of Applied Physics. 1963;**34**:3559-3567

[2] Scruby C, Dewhurst R, Hutchins D, Palmer S. Quantitative studies of thermally-generated elastic waves in laser irradiated metals. Journal of Applied Physics. 1980;**51**:6210-6216

[3] Rose LRF. Point-source representation for laser generated ultrasound. Journal of the Acoustical Society of America. 1984;**75**:723-732

[4] Doyle P. On epicentral waveforms for laser-generated ultrasound. Journal of Physics D: Applied Physics. 1986;**19**: 1613-1623

[5] McDonald F. Practical quantitative theory of photoacoustic pulse generation. Applied Physics Letters. 1989;**54**:1504-1506

[6] Spicer J. Laser Ultrasonics in finite structures: Comprehensive modeling with supportingexperiment [Ph.D. Thesis]. The Johns Hopkins University; 1991

[7] Fahmy MA. A new boundary element strategy for modeling and simulation of three temperatures nonlinear generalized micropolar-magneto-thermoelastic wave propagation problems in FGA structures. Engineering Analysis with Boundary Elements. 2019;**108**:192-200

[8] Fahmy MA. A new computerized boundary element model for three-temperature nonlinear generalized thermoelastic stresses in anisotropic circular cylindrical plate structures. In: Awrejcewicz J, Grzelczyk D, editors. Dynamical Systems Theory. London, UK: IntechOpen; 2019. pp. 1-17

[9] Fahmy MA. Boundary element model for nonlinear fractional-order heat transfer in magneto-thermoelastic FGA structures involving three temperatures. In: Ebrahimi F, editor. Mechanics of Functionally Graded Materials and Structures. London, UK: IntechOpen; 2019. pp. 1-22

[10] Fahmy MA. Boundary element mathematical modelling and boundary element numerical techniques for optimization of micropolar thermoviscoelastic problems in solid deformable bodies. In: Sivasankaran S, Nayak PK, Günay E, editors. Mechanics of Solid Deformable Bodies. London, UK: IntechOpen; 2020. pp. 1-21

[11] Fahmy MA. Boundary element modeling and optimization based on fractional-order derivative for nonlinear generalized photo-thermoelastic stress wave propagation in three-temperature anisotropic semiconductor structures. In: Sadollah A, Sinha TS, editors. Recent Trends in Computational Intelligence. London, UK: IntechOpen; 2020. pp. 1-16

[12] Fahmy MA. Boundary element algorithm for nonlinear modeling and simulation of three temperature anisotropic generalized micropolar piezothermoelasticity with memory-dependent derivative. International Journal of Applied Mechanics. 2020;**12**: 2050027

[13] Sharma N, Mahapatra TR, Panda SK. Thermoacoustic behavior of laminated composite curved panels using higher-order finite-boundary element model. International Journal of Applied Mechanics. 2018;**10**:1850017

[14] Abd-Alla AM, El-Naggar AM, Fahmy MA. Magneto-thermoelastic problem in non-homogeneous isotropic cylinder. Heat and Mass Transfer. 2003; **39**:625-629

[15] Fahmy MA. A time-stepping DRBEM for the transient

magneto-thermo-visco-elastic stresses in a rotating non-homogeneous anisotropic solid. Engineering Analysis with Boundary Elements. 2012;**36**:335-345

[16] Fahmy MA. Numerical modeling of transient magneto-thermo-viscoelastic waves in a rotating nonhomogeneous anisotropic solid under initial stress. International Journal of Modeling, Simulation, and Scientific Computing. 2012;**3**:1250002

[17] Fahmy MA. Transient magneto-thermo-viscoelastic stresses in a rotating nonhomogeneous anisotropic solid with and without a moving heat source. Journal of Engineering Physics and Thermophysics. 2012;**85**:950-958

[18] Fahmy MA. Transient magneto-thermo-elastic stresses in an anisotropic viscoelastic solid with and without moving heat source. Numerical Heat Transfer, Part A: Applications. 2012;**61**:547-564

[19] Fahmy MA. Transient magneto-thermoviscoelastic plane waves in a non-homogeneous anisotropic thick strip subjected to a moving heat source. Applied Mathematical Modelling. 2012;**36**:4565-4578

[20] Fahmy MA. The effect of rotation and inhomogeneity on the transient magneto-thermoviscoelastic stresses in an anisotropic solid. Journal of Applied Mechanics. 2012;**79**:1015

[21] Fahmy MA. A time-stepping DRBEM for magneto-thermo-viscoelastic interactions in a rotating nonhomogeneous anisotropic solid. International Journal of Applied Mechanics. 2011;**3**:1-24

[22] Fahmy MA. A Computerized Boundary Element Models for Coupled, Uncoupled and Generalized Thermoelasticity Theories of Functionally Graded Anisotropic Rotating Plates. UK: Book Publisher International; 2019

[23] Soliman AH, Fahmy MA. Range of applying the boundary condition at fluid/porous interface and evaluation of Beavers and Joseph's slip coefficient using finite element method. Computation. 2020;**8**:14

[24] Eskandari AH, Baghani M, Sohrabpour S. A time-dependent finite element formulation for thick shape memory polymer beams considering shear effects. International Journal of Applied Mechanics. 2019;**10**:1850043

[25] El-Naggar AM, Abd-Alla AM, Fahmy MA. The propagation of thermal stresses in an infinite elastic slab. Applied Mathematics and Computation. 2003;**12**:220-226

[26] El-Naggar AM, Abd-Alla AM, Fahmy MA, Ahmed SM. Thermal stresses in a rotating non-homogeneous orthotropic hollow cylinder. Heat and Mass Transfer. 2002;**39**:41-46

[27] Brebbia CA, Telles JCF, Wrobel L. Boundary Element Techniques in Engineering. New York: Springer-Verlag; 1984

[28] Wrobel LC, Brebbia CA. The dual reciprocity boundary element formulation for nonlinear diffusion problems. Computer Methods in Applied Mechanics and Engineering. 1987;**65**:147-164

[29] Partridge PW, Brebbia CA. Computer implementation of the BEM dual reciprocity method for the solution of general field equations. Communications in Applied Numerical Methods. 1990;**6**:83-92

[30] Fahmy MA. Implicit-explicit time integration DRBEM for generalized magneto-thermoelasticity problems of rotating anisotropic viscoelastic functionally graded solids. Engineering

Analysis with Boundary Elements. 2013; **37**:107-115

[31] Fahmy MA. Generalized magneto-thermo-viscoelastic problems of rotating functionally graded anisotropic plates by the dual reciprocity boundary element method. Journal of Thermal Stresses. 2013;**36**:1-20

[32] Fahmy MA. A three-dimensional generalized magneto-thermo-viscoelastic problem of a rotating functionally graded anisotropic solids with and without energy dissipation. Numerical Heat Transfer, Part A: Applications. 2013;**63**:713-733

[33] Fahmy MA. A 2-D DRBEM for generalized magneto-thermo-viscoelastic transient response of rotating functionally graded anisotropic thick strip. International Journal of Engineering and Technology Innovation. 2013;**3**:70-85

[34] Fahmy MA. A computerized DRBEM model for generalized magneto-thermo-visco-elastic stress waves in functionally graded anisotropic thin film/substrate structures. Latin American Journal of Solids and Structures. 2014;**11**:386-409

[35] Fahmy MA. A 2D time domain DRBEM computer model for magneto-thermoelastic coupled wave propagation problems. International Journal of Engineering and Technology Innovation. 2014;**4**:138-151

[36] Fahmy MA. The DRBEM solution of the generalized magneto-thermo-viscoelastic problems in 3D anisotropic functionally graded solids. In: Proceedings of the 5th International Conference on Coupled Problems in Science and Engineering (Coupled Problems 2013); 17-19 June 2013. Ibiza, Spain; 2013. pp. 862-872

[37] Fahmy MA. Boundary element solution of 2D coupled problem in anisotropic piezoelectric FGM plates. In: Proceedings of the 6th International Conference on Computational Methods for Coupled Problems in Science and Engineering (Coupled Problems 2015); 18–20 May 2015. Venice, Italy; 2015. pp. 382-391

[38] Fahmy MA. 3D DRBEM modeling for rotating initially stressed anisotropic functionally graded piezoelectric plates. In: Proceedings of the 7th European Congress on Computational Methods in Applied Sciences and Engineering (ECCOMAS 2016); 5–10 June 2016. Crete Island, Greece; 2016. pp. 7640-7658

[39] Fahmy MA. A time-stepping DRBEM for 3D anisotropic functionally graded piezoelectric structures under the influence of gravitational waves. In: Proceedings of the 1st GeoMEast International Congress and Exhibition (GeoMEast 2017); 15–19 July 2017; Sharm El Sheikh, Egypt. Facing the Challenges in Structural Engineering, Sustainable Civil Infrastructures. 2017. pp. 350-365

[40] Fahmy MA. A computerized boundary element model for simulation and optimization of fractional-order three temperatures nonlinear generalized piezothermoelastic problems based on genetic algorithm. In: AIP Conference Proceedings 2138 of Innovation and Analytics Conference and Exihibiton (IACE 2019), 25-28 March 2019. Sintok, Malaysia; 2019. p. 030015

[41] Fahmy MA. Shape design sensitivity and optimization for two-temperature generalized magneto-thermoelastic problems using time-domain DRBEM. Journal of Thermal Stresses. 2018;**41**: 119-138

[42] Fahmy MA. Boundary element algorithm for modeling and simulation of dual-phase lag bioheat transfer and biomechanics of anisotropic soft tissues.

International Journal of Applied Mechanics. 2018;**10**:1850108

[43] Fahmy MA. Shape design sensitivity and optimization of anisotropic functionally graded smart structures using bicubic B-splines DRBEM. Engineering Analysis with Boundary Elements. 2018;**87**:27-35

[44] Fahmy MA. Modeling and optimization of anisotropic viscoelastic porous structures using cqbem and moving asymptotes algorithm. Arabian Journal for Science and Engineering. 2019;**44**:1671-1684

[45] Fahmy MA. Boundary element modeling and simulation of biothermomechanical behavior in anisotropic laser-induced tissue hyperthermia. Engineering Analysis with Boundary Elements. 2019;**101**: 156-164

[46] Fahmy MA. A new LRBFCM-GBEM modeling algorithm for general solution of time fractional order dual phase lag bioheat transfer problems in functionally graded tissues. Numerical Heat Transfer, Part A: Applications. 2019;**75**:616-626

[47] Fahmy MA. Design optimization for a simulation of rotating anisotropic viscoelastic porous structures using time-domain OQBEM. Mathematics and Computers in Simulation. 2019;**66**: 193-205

[48] Fahmy MA. A new convolution variational boundary element technique for design sensitivity analysis and topology optimization of anisotropic thermo-poroelastic structures. Arab Journal of Basic and Applied Sciences. 2020;**27**:1-12

[49] Fahmy MA. Thermoelastic stresses in a rotating non- homogeneous anisotropic body. Numerical Heat Transfer, Part A: Applications. 2008;**53**: 1001-1011

[50] Abd-Alla AM, Fahmy MA, El-Shahat TM. Magneto-thermo-elastic problem of a rotating non-homogeneous anisotropic solid cylinder. Archive of Applied Mechanics. 2008;**78**:135-148

[51] Fahmy MA, El-Shahat TM. The effect of initial stress and inhomogeneity on the thermoelastic stresses in a rotating anisotropic solid. Archive of Applied Mechanics. 2008;**78**: 431-442

[52] Cattaneo C. Sur une forme de i'equation de la chaleur elinant le paradox d'une propagation instantanc. Comptes Rendus de l'Académie des Sciences. 1958;**247**:431-433

[53] Hoemmen M. Communication-Avoiding Krylov Subspace Methods. Berkeley: University of California; 2010

[54] Huang FY, Liang KZ. Boundary element method for micropolar thermoelasticity. Engineering Analysis with Boundary Elements. 1996;**17**:19-26

[55] Eringen AC. Theory of micropolar elasticity. In: Liebowitz H, editor. Fracture. Vol. II. New York: Academic Press; 1968

[56] Dragos L. Fundamental solutions in micropolar elasticity. International Journal of Engineering Science. 1984;**22**: 265-275

[57] Saad Y, Schultz MH. GMRES: A generalized minimal residual algorithm for solving nonsymmetric linear systems. SIAM Journal on Scientific and Statistical Computing. 1986;**7**:856-869

[58] Arnoldi WE. The principle of minimized iterations in the solution of the matrix eigenvalue problem. Quarterly of Applied Mathematics. 1951; **9**:17-29

[59] Lanczos C. An iteration method for the solution of the eigenvalue problem of linear differential and integral

operators. Journal of Research of the National Bureau of Standards. 1950;**45**: 255-282

[60] Pazera E, Ędrysiak J. Effect of microstructure in thermoelasticity problems of functionally graded laminates. Composite Structures. 2018; **202**:296-303

[61] Xiong QL, Tian XG. Generalized magneto-thermo-microstretch response during thermal shock. Latin American Journal of Solids and Structures. 2015; **12**:2562-2580